



Transversely optically pumped Ar:He laser with a pulsed-periodic discharge

P. A. MIKHEYEV,^{1,2} A. K. CHERNYSHOV,^{1,2} M. I. SVISTUN,¹ N. I. UFIMTSEV,¹ O. S. KARTAMYSHEVA,¹ M. C. HEAVEN,^{2,3,*} AND V. N. AZYAZOV^{1,2}

¹*P.N. Lebedev Physical institute, Samara, 443011, Russia*

²*Samara University, Samara, 443086, Russia*

³*Emory University, Atlanta, GA 30322, USA*

* mheaven@emory.edu

Abstract: Optically pumped rare gas lasers have the potential for scaling to high-power cw systems with good beam quality. Metastable atoms of heavier rare gases that are the lasing species are produced in an electric discharge at near atmospheric pressure. The key problem for this class of lasers at present is the development of a suitable discharge system. In this paper, we present the results of optimization of a pulsed discharge system with the goal of minimizing cathode sputtering and peak discharge current. The first demonstration of a transversely pumped system and measurements of the optical pumping threshold for the Ar:He laser are also presented.

© 2019 Optical Society of America under the terms of the [OSA Open Access Publishing Agreement](#)

1. Introduction

Optically pumped all-rare-gas lasers (OPRGL) [1], utilize atoms of heavier rare gases – Ne, Ar, Kr and Xe, excited in an electric discharge to the lowest in energy $1s_5$ metastable state (in Paschen notation), as lasing species. Kinetic analysis [2] showed that the laser specific output could be on the order of 10^2 W cm^{-3} with overall efficiency (including discharge requirements) as high as 60%. The pumping wavelengths for the OPRGL's are in a well-developed spectral region for laser diodes, and low spatial quality lasing from stacks of diodes can be transformed to a high-power, high quality beam. OPRGL lasing wavelengths fall in the atmospheric transparency window. For example, Ar:He lasing occurs at 912.3 nm when pumped at 811.5 nm.

Rare gas metastables host just one electron in the outermost orbital, like alkali atoms, making OPRGL kinetically analogous to the extensively studied diode pumped alkali laser (DPAL) [3]. However, OPRGL has a unique advantage – its active medium is chemically inert. Both DPAL and OPRGL are three-level systems with collisional energy transfer from the optically pumped level to the upper laser level. In an OPRGL energy transfer is efficient at an atmospheric pressure with He as the collisional partner. A complication for cesium and rubidium based DPALs is that they require light hydrocarbons to provide fast energy transfer at a moderate pressure [3]. In that case, the presence of excited alkali atoms leads to a complex chemistry that finally results in degradation of the laser medium, requiring an open-cycle gas flow in the active region.

The laser cycle is illustrated for Ar in Fig. 1, which shows both Paschen and Racah notations for the energy levels. Below, we use Paschen notation to label the electronic states of Ar atoms. Optical pumping of the $1s_5 \rightarrow 2p_9$ or $1s_5 \rightarrow 2p_8$ transition is followed by collisional energy transfer to the upper laser level $2p_{10}$ and lasing on $2p_{10} \rightarrow 1s_5$. Relaxation of the metastable $1s_5$ state occurs through $1s_4$ state, which is radiatively coupled to the ground state 1S_0 , and in collisions with rare gas atoms and impurities. For the conditions of an OPRGL the ultraviolet radiation from $1s_4$ is trapped and both channels have similar rates.

Efficient lasing of OPRGL systems requires a certain number density of metastable atoms – in the range of $10^{12} \div 10^{13} \text{ cm}^{-3}$ [2]. However, continuous production of metastable number densities in that range in the presence of $\sim 1 \text{ atm}$ of He in an electric discharge is a challenging

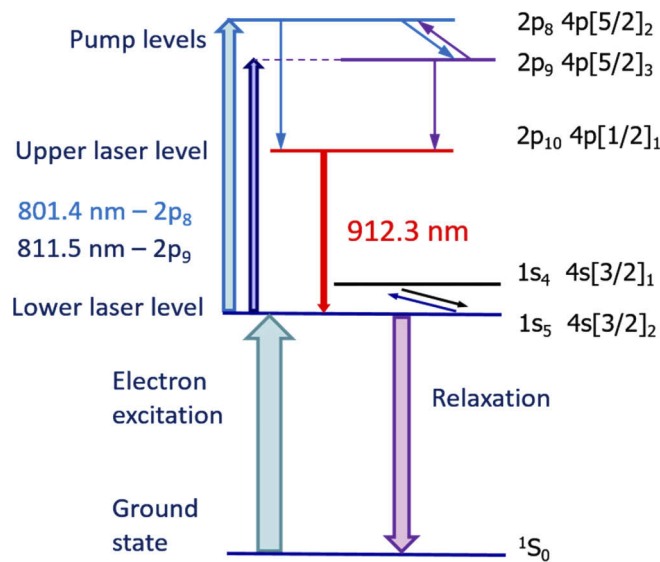


Fig. 1. Energy levels taking part in the Ar laser cycle.

task. The primary difficulty is low energy of electrons, resulting from the low value of the reduced electric field $E/N \approx 5$ Td (where E is the electric field strength, N is the particles' number density and $1\text{Td} = 10^{-17} \text{ V cm}^2$) that is sufficient to sustain continuous rare gas discharges at an atmospheric pressure. The result is a low density of the energetic electrons in the tail of their energy distribution that are above the threshold needed for excitation of metastables. As a consequence, metastable production at atmospheric pressure by continuous discharges is inefficient. CW lasing using optically pumped Ar metastables with optical-to-optical conversion efficiency of 55% was reported for a chain of continuous GHz microdischarges at atmospheric pressure [4]. However, the excited gas volume had a cross section of only 200 microns with a power density of more than 500 W cm^{-3} , and scaling of this type of discharge is unlikely. On the other hand, modeling [2] predicted a required discharge power density an order of magnitude smaller at optimal discharge conditions if $E/N \approx 10$ Td or greater could be achieved.

At present, only two types of discharges have the demonstrated potential for scaling to $E/N \geq 10$ Td in atmospheric pressure He: these are repetitively pulsed [5–7] (RPD) and dielectric barrier [8] designs. In experiments the number densities of metastables obtained in an RPD are several times larger than in a dielectric barrier discharge. Recent extensive modeling [9] for the mixture of 7% Ar in He at 270 Torr revealed that in a 20 μs pulsed discharge, E/N values in the positive column exceeded briefly 10 Td right after the beginning of the discharge pulse. But very soon, after tens of nanoseconds, E/N became as low as 4–5 Td which was insufficient for efficient Ar($1s_5$) production. The first laser experiments [1] in an excimer laser chamber utilized a pulsed 10 ns discharge that produced high enough metastables' number densities easily.

Problems with RPD arise because it requires a high peak current density for its operation, which causes noticeable cathode sputtering and complicates the design of the power supply. Atoms of the cathode material cause quenching of rare gas metastables reducing their lifetime and increasing mean discharge power needed to sustain their required number density. However, rational choice of the cathode and anode materials reduce sputtering and minimize the peak current density.

In [5], a repetitively pulsed 1300 V discharge of 80-ns duration at 200 kHz with stainless steel electrodes was realized. At He pressures up to an atmosphere the Ar($1s_5$) lifetime exceeded the

time between discharge pulses. An optically pumped laser that utilized this discharge achieved mean 3.8 W output at 12 W of absorbed continuous diode-laser pump power. This type of discharge has a macroscopic size (3 × 6 mm cross section) and the potential for scaling for larger volumes.

Another important parameter for an OPRGL system development is the pump intensity threshold. It was measured recently for Ar:He mixture in an RPD [6] and in a dielectric barrier discharge [10], for a longitudinal pumping geometry. Spectral bandwidth of the pump lasers in both experiments considerably exceeded the Ar absorption bandwidth at 811.5 nm. The objective of the experiments reported in this paper was to improve the RPD discharge system by a rational choice of the material of the electrodes, and to determine the pumping threshold of Ar:He OPRGL in a transverse pumping geometry, using a narrow-band radiation of a dye laser. The data obtained from these measurements are well-suited for the development and evaluation of computational models for the Ar:He laser. As pulsed optical excitation was applied (with a low duty cycle) the system can be modeled without the complications of accounting for the heat and mass transfer caused by the optical excitation.

Transverse optical pumping of an OPRGL has been modeled previously [11], but the present work is the first experimental study of this configuration. We show that the metastable number densities needed to utilize the shorter optical pump path of the transverse geometry are achievable. This is a significant advance as it is likely that high-powered devices will employ transverse pumping [11].

2. Experiment

The RPD discharge setup consisted of a pair of metal 4 × 15 mm electrodes with 3 mm discharge gap mounted inside a vacuum chamber that consisted of a 6-way cross sealed with KF50 flanges. One of the electrodes was connected to the cross body and another one at the opposite flange was isolated, and 80 ns FWHM current pulses from a laboratory-made power supply were fed to it through a 50 Ohm coaxial cable. The body of the 6-way cross was electrically isolated from ground. This arrangement reduced stray interference from discharge current pulses.

The other four KF flanges were equipped with quartz windows mounted at Brewster angles to corresponding optical axes. Probe radiation for measurements of metastable number densities and lifetime, as well as pump radiation for experiments with lasing were directed along the 4 mm side of the electrodes perpendicularly to lasing optical axis (transverse optical pumping).

The vacuum system included an oil-free scroll pump and Bronkhorst flow meter with a metering valve for He, and Bronkhorst flow controller for Ar, providing 2 slpm flow rate. He and Ar gases were of 6.0 purity from Linde.

Measurements of [Ar(1s₅)] number density and lasing experiments were performed using a 200 kHz discharge pulse repetition rate. To measure [Ar(1s₅)] and metastables lifetime, a laboratory made tunable diode laser [12] provided the CW probe radiation, which was detected by a photodiode with 0.8 μs time response. Detailed description of the experimental setup for [Ar(1s₅)] measurements was reported in [13,14]. The absorption profile of the 4s[3/2]₂ → 4p[5/2]₃ transition (1s₅ → 2p₉ in Paschen notation) was fitted to a Lorentz function, as the Gaussian component was negligible in the presence of He at pressures near 1 atm. The discharge conditions used produced [Ar(1s₅)] ≈ 10¹³ cm⁻³, resulting in opaque samples if the probe laser was tuned to the line center. To avoid incorrect interpretation of the data recorded in the opaque range, the central part of the absorption profile was excluded from the fit. The time needed for one frequency scan of the tunable diode laser was 40 ms, allowing for measurements of the mean value of [Ar(1s₅)]. However, as time-resolved measurements revealed, at 200 kHz changes in [Ar(1s₅)] were only about 20% over the time between discharge pulses.

For time-resolved measurements, the laser was detuned approximately 5 GHz away from the 811.5 nm line center to avoid saturation, and operated at a constant wavelength. Evolution of the

absorption by Ar(1s₅) was recorded by a digital oscilloscope and further processed with the help of Origin software.

A pulsed tunable dye laser was used as the pump source for the lasing experiments. This system consisted of a frequency-doubled Nd/YAG laser (Quanta Ray Pro) that pumped a Sirah Precision Scan dye laser. The bandwidth of the dye laser as stated by the manufacturer was 1 GHz. It was necessary to synchronize the pump laser pulse with the discharge current pulse so that lasing occurred at the same discharge conditions with the same [Ar(1s₅)]. A Stanford Research Systems DG645 delay generator triggered by the discharge was used to trigger the Nd/YAG laser at a rate of 10 Hz, with a constant delay between the preceding discharge excitation and the dye laser pulse. The 10 Hz timing pulses were also used to trigger an Avantes fiber-coupled spectrometer (AvaSpec-2048), ensuring capture of each of OPRGL output pulse. The laser resonator consisted of two plain mirrors separated by ~50 cm. The output mirror transmission, used for the determination of lasing threshold, was specified by the manufacturer to be 5%.

A schematic of the experimental setup is represented in Fig. 2. The dye laser beam was 6 mm in diameter with a nearly flat transverse intensity distribution. This beam was passed through a $\times 3$ beam expander followed by a $\times 6$ cylindrical collimating lens to produce an elliptical beam 18 \times 3 mm in size, confirmed by the burn mark on thermal paper.

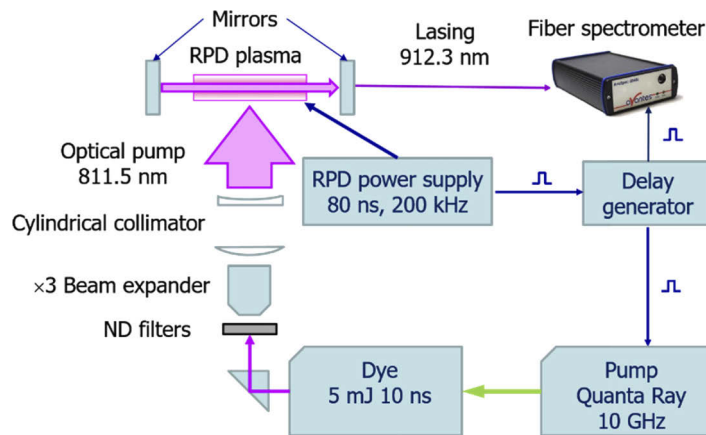


Fig. 2. Schematics of the experimental setup for the experiments with lasing

To determine lasing threshold, the pump beam energy was attenuated with the help of a set of Thorlabs neutral density filters. The data for the filters' transmission at 811.5 and 801.4 nm was obtained from the Thorlabs website. Pump laser energy was measured by an Ophir PE50 BF-C pyroelectric energy sensor.

3. Results

Cathode sputtering in an RPD decreases the lifetime of rare gas metastables. Excitation energy of their 1s₅ states is on the order of 10 eV, providing high probability for ionization of any stray atoms or molecules via collisions [15]. There are also inherent processes that cause loss of Ar metastables in a high-pressure He bath like excimer formation, transfer to the Ar(1s₄) state and quenching to the ground state. Data on sputtering phenomena [16] suggests that metals like Ti or W demonstrate considerably lower sputtering yields compared to stainless steel used in the earlier experiments [5,6]. However, cathode material may affect discharge stability and normal cathode current density – the current density when a cathode surface becomes completely enveloped by the discharge. Therefore, experiments were necessary to compare the performance of electrodes manufactured from different metals.

We tested a number of cathode-anode pairs, manufactured from stainless steel, aluminum, titanium, copper and tungsten in attempt to find electrodes best suited for our task. Discharge stability, homogeneity, and minimal cathode normal current density were the performance criteria examined. All tested configurations could provide $[Ar(1s_5)] \approx 10^{13} \text{ cm}^{-3}$, but we found that a tungsten (W) cathode and electrochemically platinum (Pt) covered titanium (Ti) anode exhibited the best performance. With this combination of materials, the normal current density was less than 3 A cm^{-2} at the current peak. We performed all of the experiments described below with this pair of electrodes for a mixture of 1% Ar in He. The peak current density was 3 A cm^{-2} , which was $\sim 10\%$ larger than normal current density. Note that for stainless steel electrodes, the normal current density was as high as 10 A cm^{-2} .

After each pair of electrodes under study was assembled inside the discharge chamber, we allowed the discharge to operate for 4 hours in pure He at a pressure of 250 Torr and at low current, sufficient to condition the electrodes' surfaces, then evacuated the chamber until the next day. Then, when we operated the discharge for 2 hours and after that, the discharge in Ar:He mixtures became stable up to 750 Torr. After the discharge operated for a few weeks, we observed further discharge improvement. Homogeneous discharge could be sustained up to 850 Torr and further increase in pressure was limited by the discharge chamber design. Only after this period of discharge operation, we performed all the measurements reported below.

Figure 3 shows typical traces of discharge current, voltage and their product – discharge power.

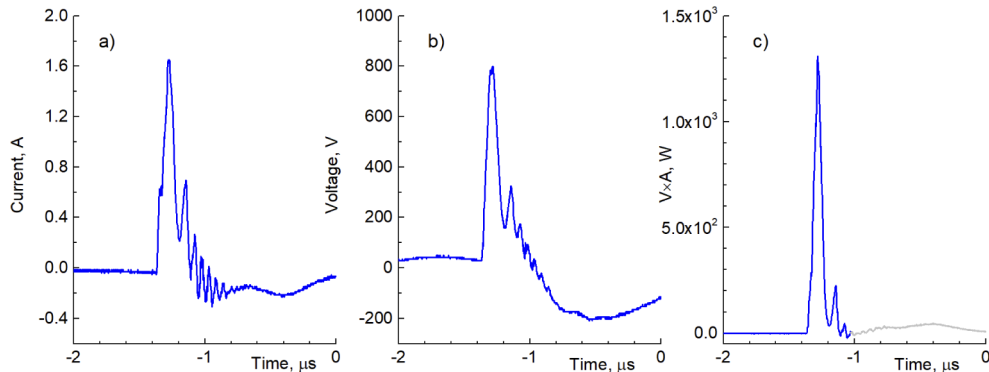


Fig. 3. Traces of discharge current a), voltage b) and their product – discharge power c).

Only the dark part of the power trace was integrated to determine energy deposited in the discharge. 1% Ar in He at 700 Torr. W cathode, Pt covered Ti anode. Energy load is $1 \times 10^{-4} \text{ J}$.

Poor matching is evident due to use of a 50 Ohm cable to power the discharge with an order of magnitude larger impedance. However, we still could estimate energy input into the discharge by integrating the blue region of the trace in Fig. 3(c). Energy of one discharge pulse determined by this analysis was about $100 \mu\text{J}$ and we kept it constant in our experiments, because a further increase in energy did not produce a substantial increase in $[Ar(1s_5)]$.

Typical results of measurements of the $[Ar(1s_5)]$ temporal profile at 800 Torr for the tungsten cathode and titanium anode electrochemically covered by platinum are represented in Fig. 4. The upper trace in Fig. 4(a) is the temporal evolution of the probe laser absorption between discharge pulses with the probe detuned from the center of the $Ar(1s_5)$ absorption line at 811.5 nm. In this particular case, the time interval between pulses was set to $5 \mu\text{s}$ to provide conditions typical for an OPRGL operation. The trace shows that decrease in $[Ar(1s_5)]$ between discharge pulses was only 20%.

The lower trace in Fig. 4(a) is the logarithm of the dark part of the upper trace in Fig. 4(a). Evidently, the dark part of the lower trace was linear, demonstrating true exponential decay, and

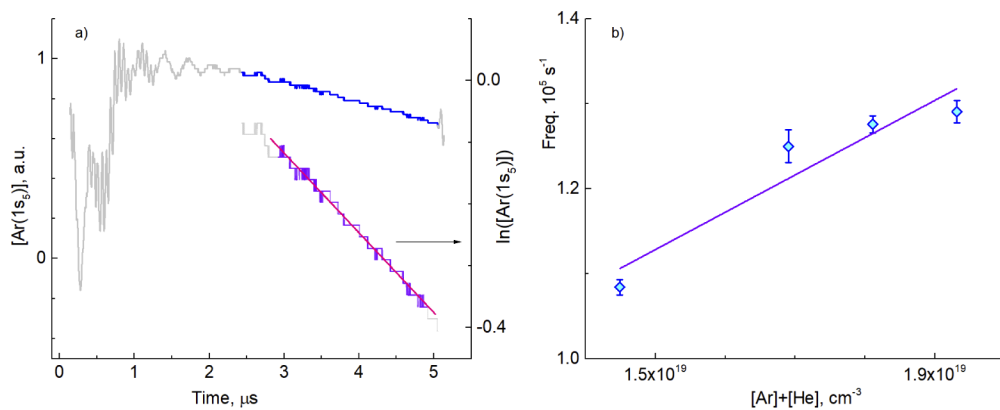


Fig. 4. Traces of $[\text{Ar}(1s_5)]$ and $\ln([\text{Ar}(1s_5)])$ that demonstrates its linear portion (dark part of the curve), used to determine kinetic frequency and lifetime at 800 Torr –(a); quenching frequency of $\text{Ar}(1s_5)$ vs gas mixture number density with account for temperature deduced from the absorption line shape –(b). 1% Ar in He mixture; W cathode, Pt covered Ti – anode.

the kinetic frequency and lifetime were determined from that part. The lifetime at 800 Torr was 8 μs .

The loss frequencies in our experiments were on the order of 10^5 s^{-1} near atmospheric pressure. Quenching rate constant deduced from the slope of the linear fit in Fig. 4(b) amounts to $(5 \pm 1) \times 10^{-15} \text{ cm}^3 \text{ s}^{-1}$. Rate constant for $\text{Ar}(1s_5)$ quenching to the ground state ${}^1\text{S}_0$ by He $(2.4 \pm 0.3) \times 10^{-15} \text{ cm}^3 \text{ s}^{-1}$ was recently measured using e-beam discharge techniques [17]. There is another channel of energy transfer from $\text{Ar}(1s_5)$ state – to the $\text{Ar}(1s_4)$ and back with room temperature rate constants of $(2.1 \pm 0.2) \times 10^{-15} \text{ cm}^3 \text{ s}^{-1}$ [18] and $(1 \pm 0.3) \times 10^{-13} \text{ cm}^3 \text{ s}^{-1}$ [19], respectively. $\text{Ar}(1s_4)$ is radiatively coupled to the ground state and has a lifetime of 7.6 ns, but in the OPRGL conditions this radiation is trapped leading to the effective lifetime on the order of microseconds [20]. Using these data we can estimate the frequency for the $1s_5$ loss through $1s_4$ under the conditions of our experiment to be in the range $(1 \div 2) \times 10^4 \text{ s}^{-1}$ and frequency for quenching to the ground state is about $5 \times 10^4 \text{ s}^{-1}$. Both channels have linear dependence on He number density, but somewhat smaller sum frequency compared to the results shown in Fig. 4(b). This suggests presence of quenching by some contamination in the laser medium due to sputtering or quality of the gases.

In Fig. 5 the dependences of $[\text{Ar}(1s_5)]$ and Lorentzian linewidth WL of 811.5 nm line on pressure are represented. Linewidths at 300 K for the studied pressure range are plotted for reference. $[\text{Ar}(1s_5)]$ exhibited weak dependence on pressure, being near 10^{13} cm^{-3} . The discharge energy load was almost constant and near 10^{-4} J per pulse. There was a noticeable difference in WL measured in the experiment, and calculated for room temperature, providing a way to assess the mean temperature in the discharge region. The pressure broadening coefficient at 300 K for the 811.5 nm Ar line measured in [13,14] is $3.4 \times 10^{-10} \text{ s}^{-1} \text{ cm}^{-3}$ and has a $T^{0.3}$ temperature dependence. Using this data, we could estimate temperature to be $\sim 400 \text{ K}$ in the discharge excited gas.

At 700 Torr the measured peak voltage of the discharge pulse for 3 mm discharge gap amounted to 795 V. Bearing in mind that the cathode fall in such a discharge is $\sim 300 \text{ V}$ we could estimate the reduced electric field E/N at 700 Torr to be near 10 Td, which is optimal for metastable production.

In our experiments the discharge volume was $0.4 \times 1.5 \times 0.3 = 0.18 \text{ cm}^3$. The energy stored in that volume by the $1s_5$ state for $[\text{Ar}(1s_5)] = 10^{13} \text{ cm}^{-3}$ is $3.3 \mu\text{J}$. Taking into account that at least half of the energy deposited into discharge ($100 \mu\text{J}$) goes into the positive column (the other part

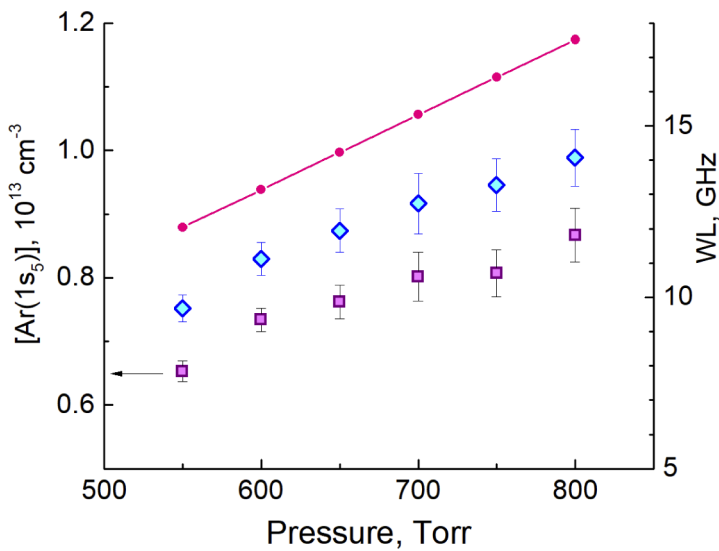


Fig. 5. Dependences of $[\text{Ar}(1s_5)]$ (squares) and 811.5 nm Lorentian linewidth WL (rhombuses) on pressure. Filled circles connected with a straight line are the calculated values of linewidth at 300 K.

heats the electrodes due to energy release in the electrode layers) we obtain discharge efficiency of $\sim 7\%$ – in good agreement with the value predicted in [2].

Experiments with transverse optical pumping by a narrow band dye laser showed that lasing in the Ar:He mixture could be produced easily. Figure 6 is a plot of OPRGL output energy against mean pump intensity. The lasing threshold was measured several times and found to be $250 \pm 150 \text{ W cm}^{-2}$ for $2p_9$ and $700 \pm 200 \text{ W cm}^{-2}$ for $2p_8$. Hence, it was possible to pump the Ar OPRGL through $2p_8$ state at 801.4 nm, but the pumping threshold determined for this level was three times larger than that of $2p_9$. Experimental uncertainty mostly originated from the crude determination of the pump radiation area in the discharge region and uncertainty in the pump pulse duration ($\sim 10 \text{ ns}$). The two sets of markers in Fig. 6(a) represent results obtained after realignment of all optical components, permitting an assess of the experimental uncertainty.

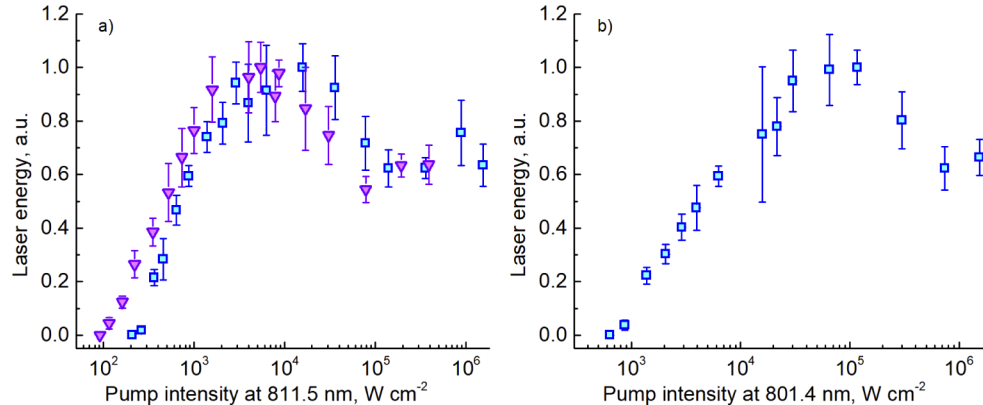


Fig. 6. Laser pulse energy against pump intensity: pump levels are $2p_9$ – a) and $2p_8$ – b). Triangles on a) are data obtained after realignment of the optical setup.

With the present experimental configuration we found that the threshold for $2p_9$ pumping was an order of magnitude smaller than was measured in [10] with a broadband pump (~ 30 GHz) in a dielectric barrier discharge and longitudinal pumping configuration.

The plots of laser output exhibited saturation and then an unexpected roll-off with increasing pump intensity for pumping of both levels. Saturation occurred at ~ 10 kW cm $^{-2}$ for the $2p_9$ level and at ~ 100 kW cm $^{-2}$ for the $2p_8$ level. The cause of saturation is bleaching of the active medium – the bottleneck of the system, when energy transfer rate to the upper laser level is slower than pumping rate. The reason for the roll-off is not clear yet and needs further investigation.

4. Conclusion

Experiments with repetitively pulsed discharge revealed the importance of rational choice of the materials for the cathode and anode. Optimal materials reduce the peak discharge current and cathode sputtering, increasing discharge efficiency of metastable production. The number density [$\text{Ar}(1s_5)$] = 10^{13} cm $^{-3}$ produced in this type of discharge is quite sufficient for efficient laser operation.

The measured metastable quenching frequency or lifetime in our experiments was quite close, but somewhat larger than predicted from known kinetic data. The discrepancy may arise from impurities in the reagent gases and cathode sputtering, as well as from unknown temperature dependence of the rate constants.

The measured pumping threshold for pumping of the $2p_9$ state was 250 ± 150 W cm $^{-2}$, and 700 ± 200 W cm $^{-2}$ for pumping to $2p_8$. Previously, in the longitudinal pumping configuration with a broadband pump laser (~ 30 GHz) [10] the measured threshold for $2p_9$ was 3.9 kW cm $^{-2}$. Pumping thresholds were also measured in experiments with a CW pumping in longitudinal configurations. For a diode laser pump [6] the threshold amounted to 590 W cm $^{-2}$, and in experiments with a narrowband (< 2 GHz) TiSa laser [4] it was ~ 500 W cm $^{-2}$. Theoretical estimations [21] predicted pumping threshold in a longitudinal configuration in the range 400-600 W cm $^{-2}$. Larger values of threshold in longitudinal configurations seems reasonable because of an unfavorable longitudinal distribution of gain, compared to transverse pumping.

The decrease in laser output with pump power in an OPRGL was not observed before, its physical reason is not clear yet and needs further investigation.

Funding

Ministry of Education and Science of the Russian Federation (3.1715.2017/4.6).

Disclosures

The authors declare no conflicts of interest.

References

1. J. Han and M. C. Heaven, "Gain and lasing of optically pumped metastable rare gas atoms," *Opt. Lett.* **37**(11), 2157–2159 (2012).
2. A. V. Demyanov, I. V. Kochetov, and P. A. Mikheyev, "Kinetic study of a cw optically pumped laser with metastable rare gas atoms produced in an electric discharge," *J. Phys. D: Appl. Phys.* **46**(37), 375202 (2013).
3. W. F. Krupke, "Diode pumped alkali lasers (DPALs)—A review," *Prog. Quantum Electron.* **36**(1), 4–28 (2012).
4. W. T. Rawlins, K. L. Galbally-Kinney, S. J. David, A. R. Hoskinson, J. A. Hopwood, and M. C. Heaven, "Optically pumped microplasma rare gas laser," *Opt. Express* **23**(4), 4804 (2015).
5. J. Han, M. C. Heaven, P. J. Moran, G. A. Pitz, E. M. Guild, C. R. Sanderson, and B. Hokr, "Demonstration of a CW diode-pumped Ar metastable laser operating at 4 W," *Opt. Lett.* **42**(22), 4627 (2017).
6. J. Han, M. C. Heaven, P. J. Moran, G. A. Pitz, E. M. Guild, C. R. Sanderson, and B. Hokr, "Pulsed discharge - diode pumped Ar* Laser," *J. Directed Energy* **6**, 209–219 (2017).
7. P. Sun, D. Zuo, P. A. Mikheyev, J. Han, and M. C. Heaven, "Time-dependent simulations of a CW pumped, pulsed DC discharge Ar metastable laser system," *Opt. Express* **27**(16), 22289–22301 (2019).

8. P. A. Mikheyev, J. Han, A. Clark, C. Sanderson, and M. C. Heaven, "Production of Ar and Xe metastables in rare gas mixtures in a dielectric barrier discharge," *J. Phys. D: Appl. Phys.* **50**(48), 485203 (2017).
9. D. J. Emmons and D. E. Weeks, "Kinetics of high pressure argon-helium pulsed gas discharge," *J. Appl. Phys.* **121**(20), 203301 (2017).
10. P. A. Mikheyev, J. Han, and M. C. Heaven, "Lasing in optically pumped Ar:He mixtures excited in a dielectric barrier discharge," *Proc. SPIE* **11042**, 1104206 (2019).
11. J. Gao, Y. He, P. Sun, Z. Zhang, X. Wang, and D. Zuo, "Simulations for transversely diode-pumped metastable rare gas lasers," *J. Opt. Soc. Am. B* **34**(4), 814–823 (2017).
12. A. K. Chernyshov, P. A. Mikheyev, and N. N. Lunev, "Diode laser with external double reflector for gas analysis," *Bull. Lebedev Phys. Inst.* **45**(3), 83–86 (2018).
13. P. A. Mikheyev, A. K. Chernyshov, N. I. Ufimtsev, E. A. Vorontsova, and V. N. Azyazov, "Pressure broadening of Ar and Kr $(n+1)s[3/2]2 \rightarrow (n+1)p[5/2]3$ transition in the parent gases and in He," *J. Quant. Spectrosc. Radiat. Transfer* **164**, 1–7 (2015).
14. A. K. Chernyshov, P. A. Mikheyev, and N. I. Ufimtsev, "Measurement of pressure shift and broadening for Ar and Kr $4s[3/2]2 \rightarrow 4p[5/2]3$ transition in rare gases using diode-laser spectroscopy," *J. Quant. Spectrosc. Radiat. Transfer* **222-223**, 84–88 (2019).
15. L. G. Piper, J. E. Velasco, and D. W. Setser, "Quenching cross sections for electronic energy transfer reactions between metastable argon atoms and noble gases and small molecules," *J. Chem. Phys.* **59**(6), 3323–3340 (1973).
16. K. Wasa, "Sputtering Phenomena," in *Handbook of Sputtering Technology*, 2nd ed. (William Andrews Publishing, Norwich, 2012), pp. 41–75.
17. A. A. Ionin, I. V. Kholin, A. Y. L'Dov, L. V. Seleznev, N. N. Ustinovskii, and D. A. Zayarnyi, "On the possibility of developing quasi-CW high-power high-pressure laser on 4p-4s transition of Ar I with electron beam-optical pumping: quenching of 4s (3P_2) lower laser level," *Laser Phys.* **27**(12), 125803 (2017).
18. V. A. Ivanov, I. V. Makasyuk, and A. S. Prikhod'ko, "Collisional destruction of argon 4s(3P_2) metastable atoms in a helium-argon mixture," *Optika i Spektroskopiya* **72**, 290–292 (1992).
19. J. Han and M. C. Heaven, "Kinetics of optically-pumped Ar metastables," *Opt. Lett.* **39**(22), 6541–6544 (2014).
20. K. Igarashi, S. Mikoshiba, Y. Watanabe, M. Suzuki, and S. Murayama, "Characterization of imprisoned Xe resonant photons in He-Xe and Ne-Xe," *J. Phys. D: Appl. Phys.* **28**(7), 1377–1383 (1995).
21. B. Eshel and G. P. Perram, "Five-level argon-helium discharge model for characterization of a diode-pumped rare-gas laser," *J. Opt. Soc. Am. B* **35**(1), 164–173 (2018).